Supporting Information

Donor−Acceptor-Appended Triarylboron Lewis Acids: Ratiometric or Time-Resolved Turn-On Fluorescence Response toward Fluoride Binding

Heechai Lee,[†] Saibal Jana,[§] Juhee Kim,[†] Sang Uck Lee,[‡,*] and Min Hyung Lee[†,*]

[†] *Department of Chemistry, University of Ulsan, Ulsan 44610, Republic of Korea*

[‡] *Department of Bionano Technology and Department of Chemical and Molecular Engineering, Hanyang University, Ansan 15588, Republic of Korea*

[§] *Department of Chemistry, University of Liverpool, Crown Street, Liverpool, L69 7ZD, United Kingdom*

* E-mail: sulee@hanyang.ac.kr; lmh74@ulsan.ac.kr

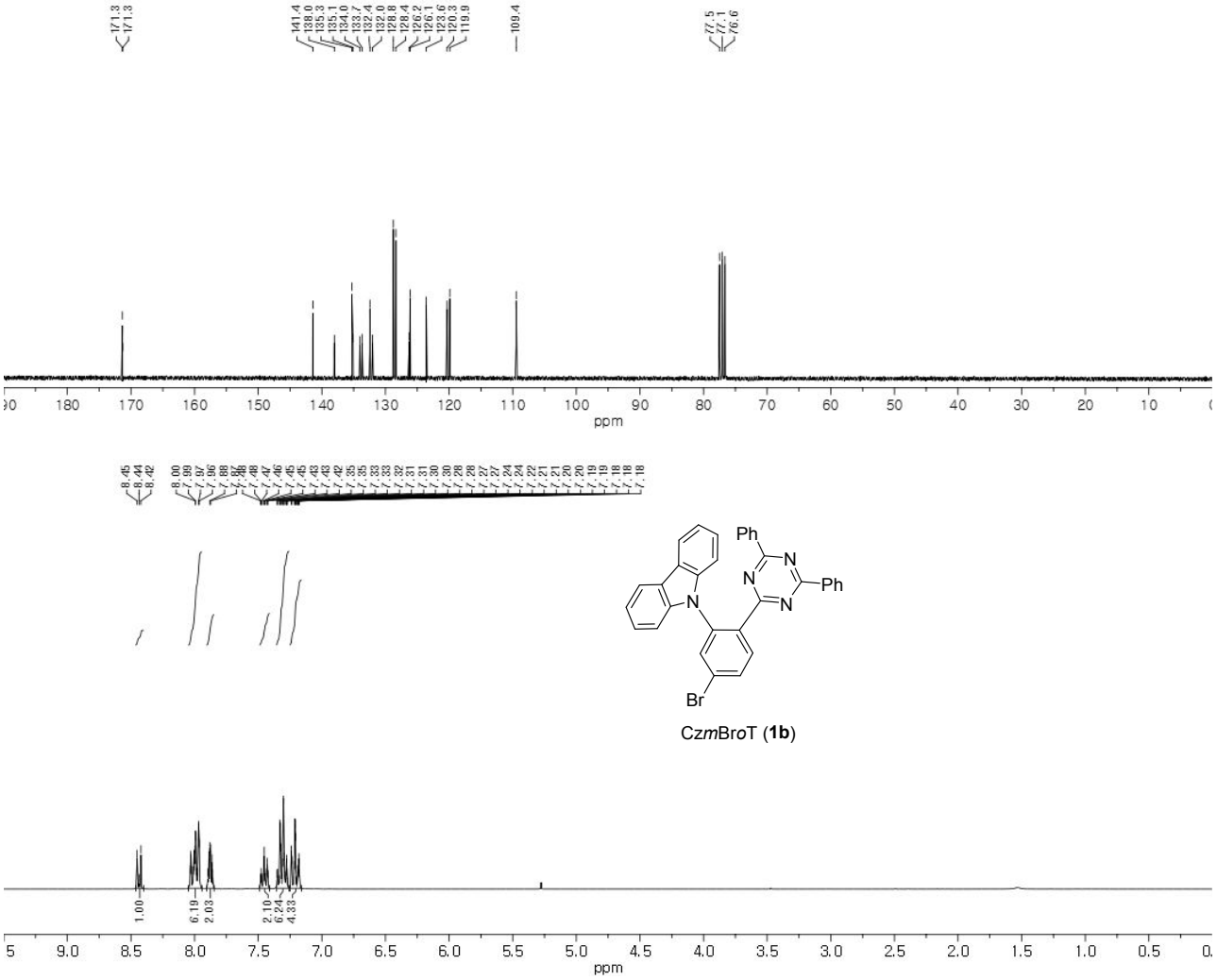

Figure S1. ^{1}H (bottom) and ^{13}C (top) NMR spectra of **1b** in $CDCl_3$.

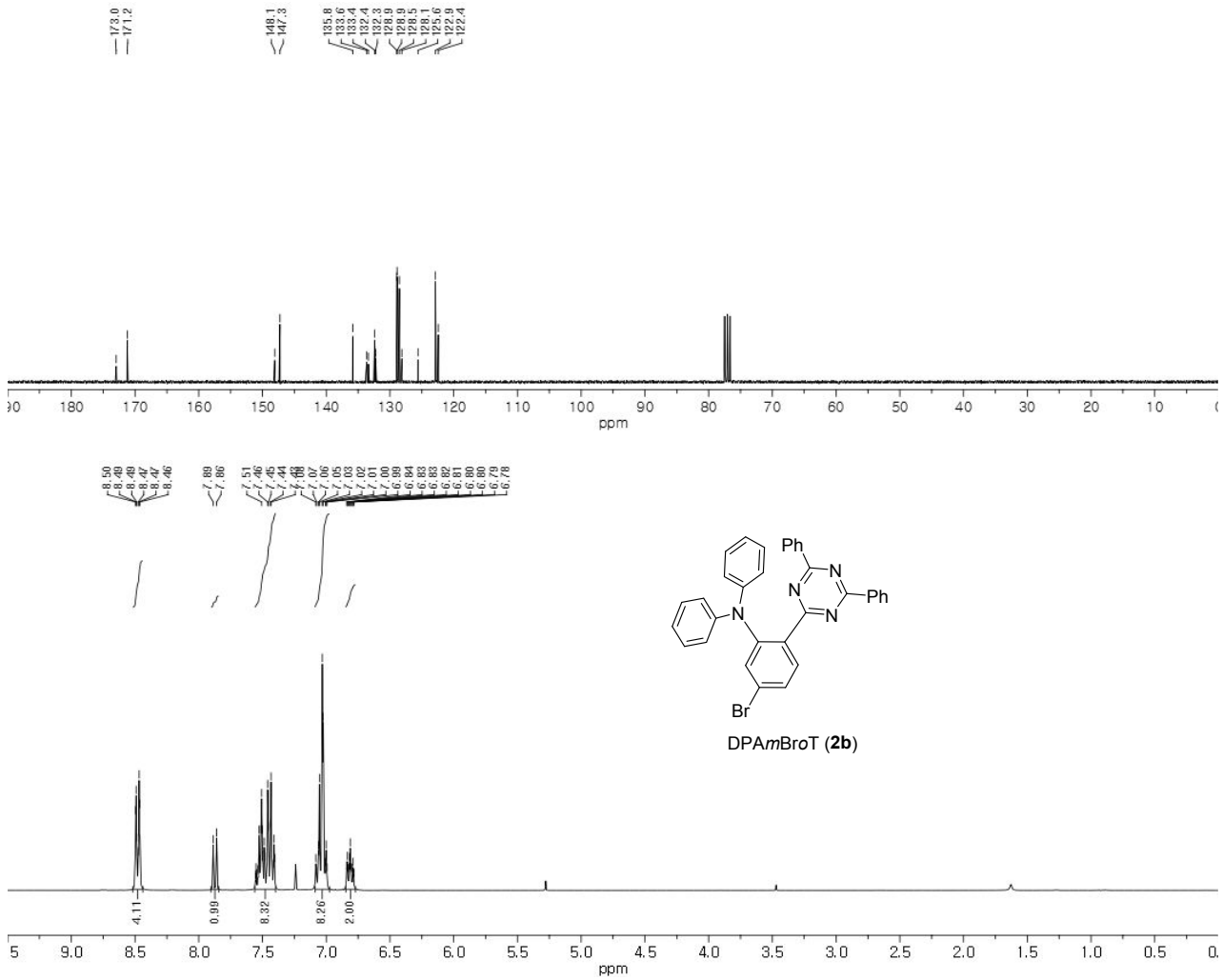

Figure S2. ^{1}H (bottom) and ^{13}C (top) NMR spectra of **2b** in $CDCl_3$.

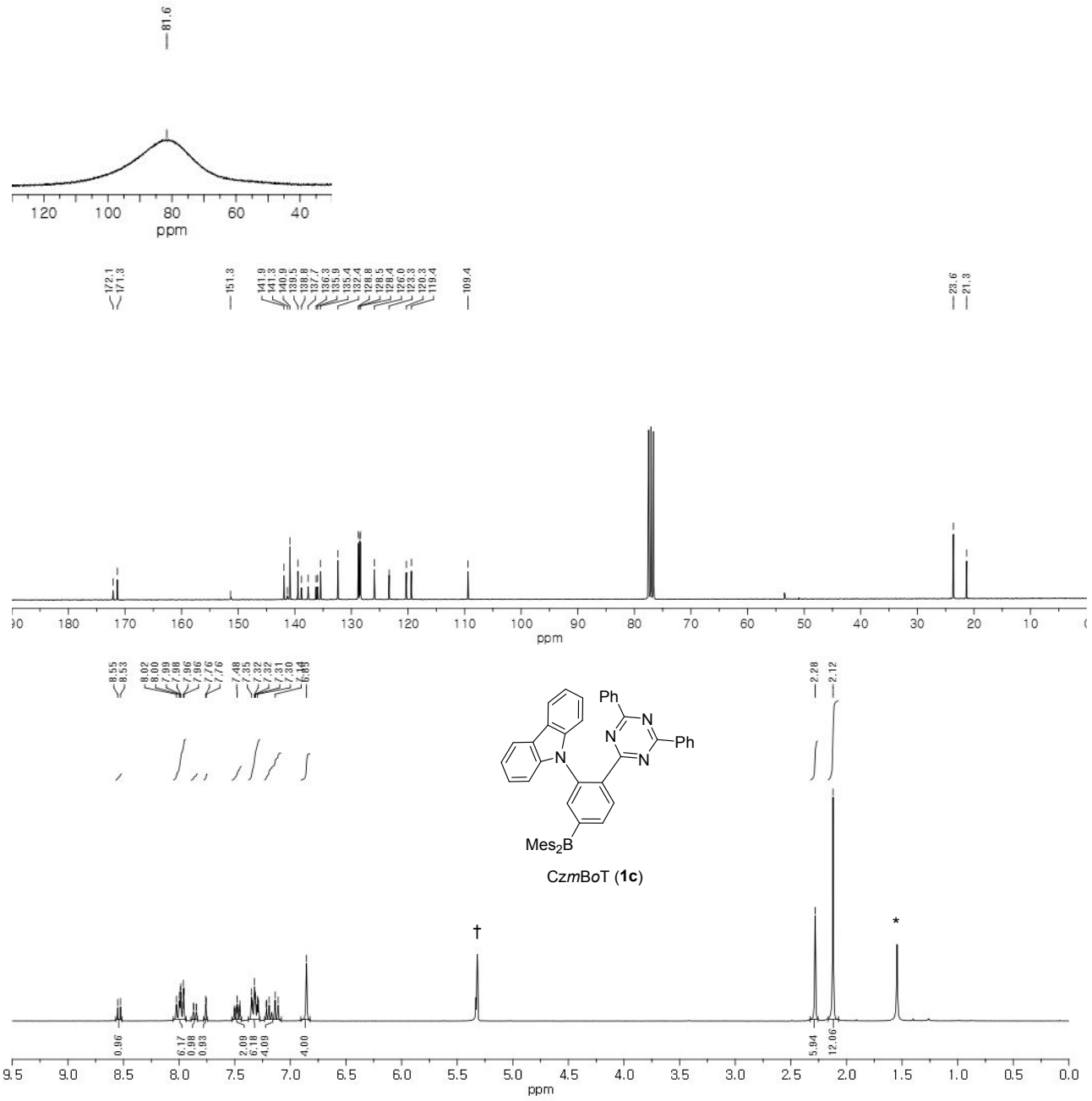

Figure S3. ^{1}H (bottom), ^{13}C (middle), and ^{11}B (top) NMR spectra of **1c** in CD_2Cl_2 ($CDCl_3$ for ^{13}C NMR; * from residual H_2O, † from CH_2Cl_2).

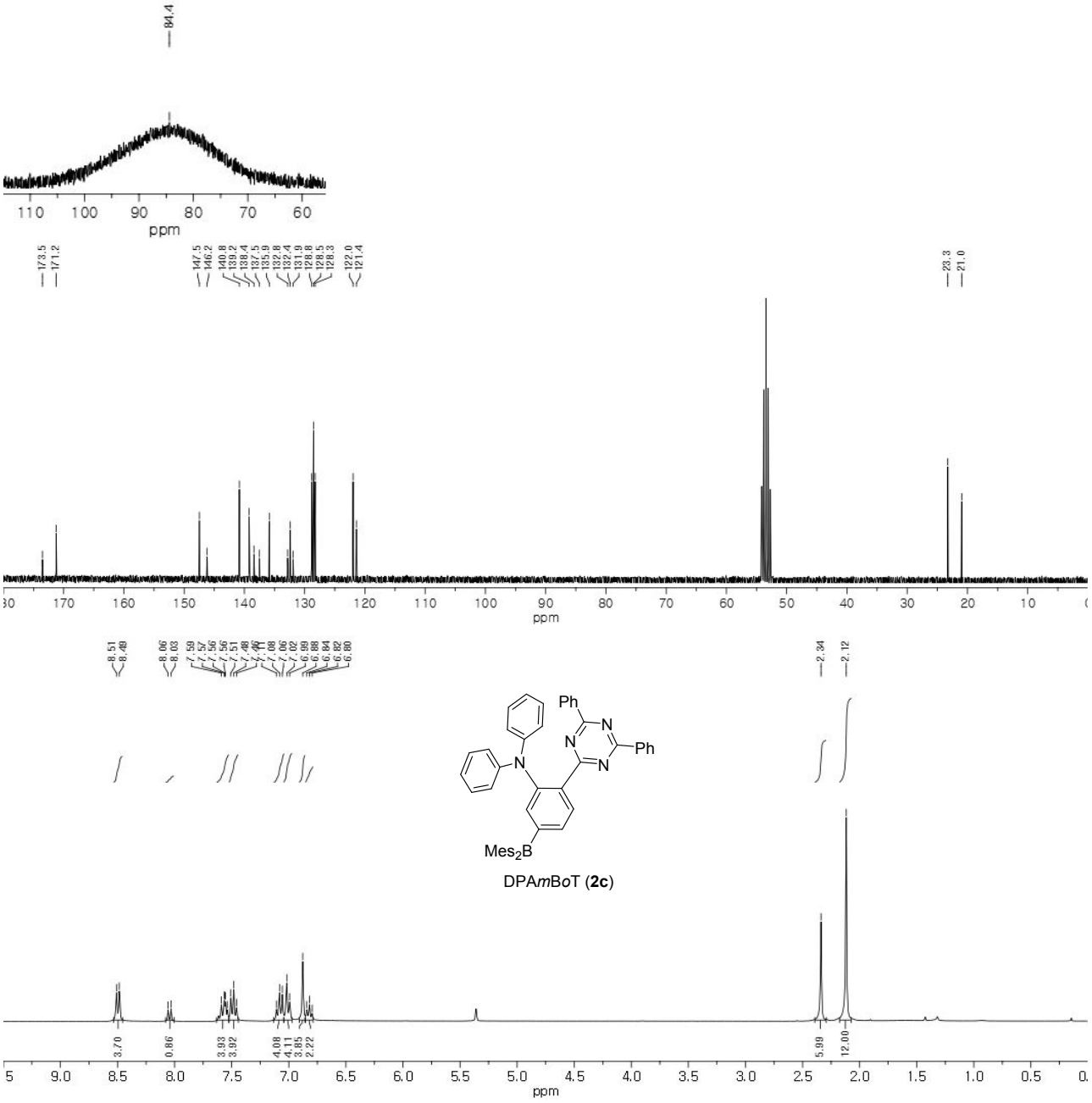

Figure S4. ^{1}H (bottom), ^{13}C (middle), and ^{11}B (top) NMR spectra of **2c** in CD_2Cl_2.

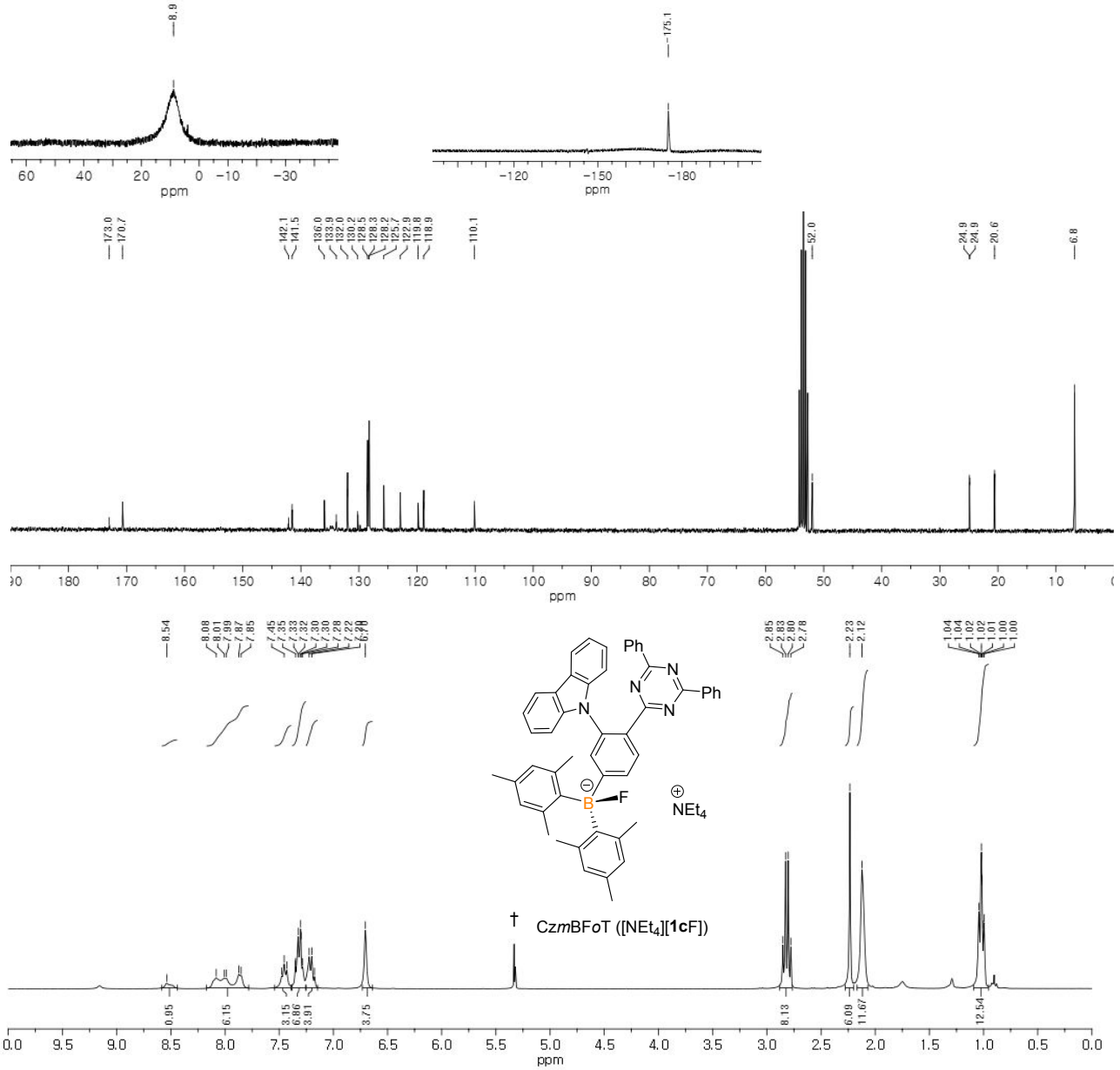

Figure S5. ^{1}H (bottom), ^{13}C (middle), ^{11}B (top left), and ^{19}F (top right) NMR spectra of [NEt_4][**1c**F] in CD_2Cl_2 († from residual CH_2Cl_2).

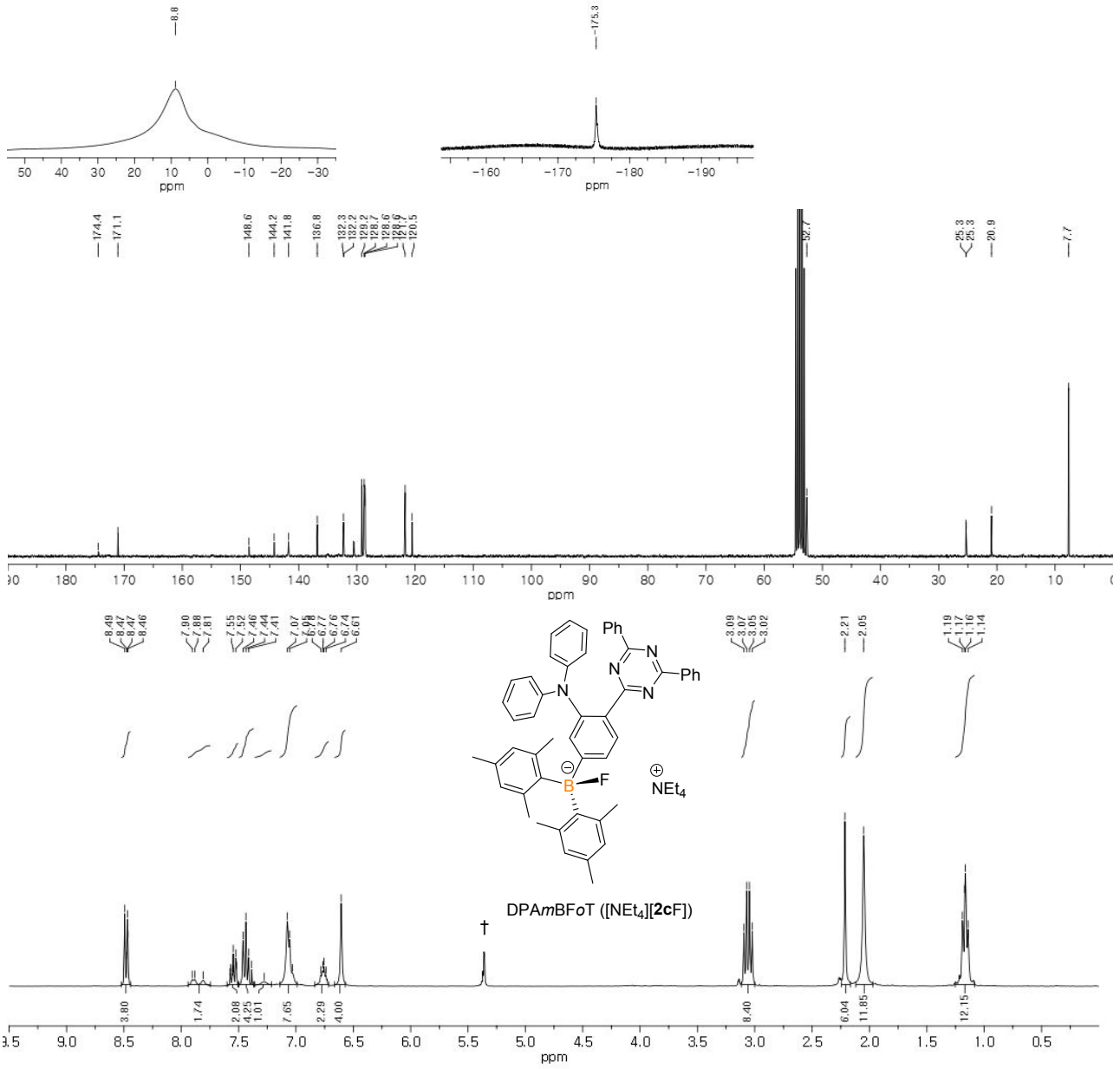

Figure S6. ^{1}H (bottom), ^{13}C (middle), ^{11}B (top left), and ^{19}F (top right) NMR spectra of [NEt_4][**2c**F] in CD_2Cl_2 († from residual CH_2Cl_2).

X-ray Data Collection and Refinement Details.

Single crystals of [NEt_4][**1c**F] were coated with Paratone oil and mounted onto a glass capillary. The crystallographic measurements were performed on a Bruker SMART Apex II CCD area detector diffractometer with a graphite-monochromated Mo-Kα radiation (λ = 0.71073 Å) at 296 K. The structures were solved by direct methods[1] and refined by full-matrix least-squares fitting on F^2 using the SHELXL-2014.[2] All non-hydrogen atoms were refined with anisotropic displacement parameters. Hydrogen atoms were placed at their geometrically calculated positions and were refined riding on the corresponding carbon atoms with isotropic thermal parameters. CCDC No. 1949639 contains the supplementary crystallographic data for this paper. The data can be obtained free of charge from The Cambridge Crystallographic Data Centre via www.ccdc.cam.ac.uk/structures.

1. G.M. Sheldrick, SHELXS-97: Program for the Solution of Crystal Structures, University of Göttingen, Germany, 2008.
2. G.M. Sheldrick, SHELXL-2014: Program for Crystal Structure Refinement, University of Göttingen, Germany, 2014.

Table S1. Crystallographic data and parameters for [NEt_4][**1c**F].

	[NEt_4][**1c**F]
formula	$C_{59}H_{63}BFN_5$
formula weight	871.95
crystal system	Monoclinic
space group	$P2_1/c$
a (Å)	15.6211(5)
b (Å)	11.5988(4)
c (Å)	27.1934(9)
α (°)	90
β (°)	102.065(2)
γ (°)	90
V (Å^3)	4818.2(3)
Z	4
ρ_{calc} (g cm^{-3})	1.202
μ (mm^{-1})	0.073
F(000)	1616
T (K)	296(2)
hkl range	−18 → +18, −13 → +13, −28 → +32
measd reflns	61676
unique reflns [R_{int}]	8825 [0.1380]
reflns used for refinement	8825
refined parameters	605
R1[a] (I > 2σ(I))	0.0619
wR2[b] all data	0.1890
GOF on F^2	0.939
ρ_{fin} (max/min) (e Å^{-3})	0.237/−0.251

[a] $R1 = \sum||Fo| - |Fc||/\sum|Fo|$. [b] $wR2 = \{[\sum w(Fo^2 - Fc^2)^2]/[\sum w(Fo^2)^2]\}^{1/2}$.

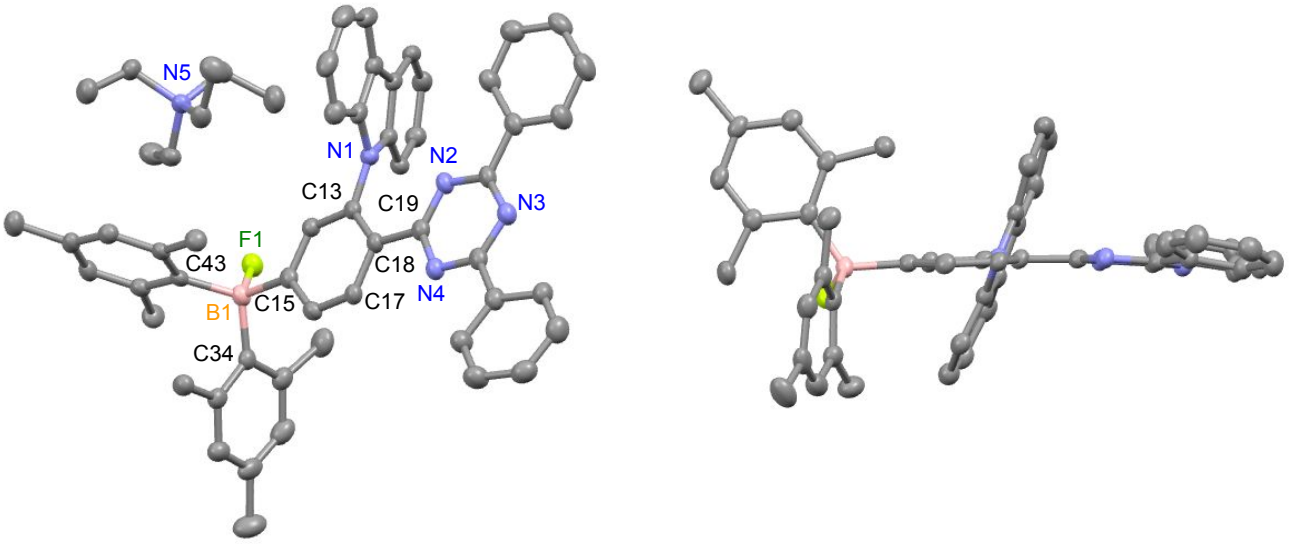

Figure S7. X-ray crystal structure of [NEt_4][**1c**F] (50% thermal ellipsoids). The H atoms are omitted for clarity.

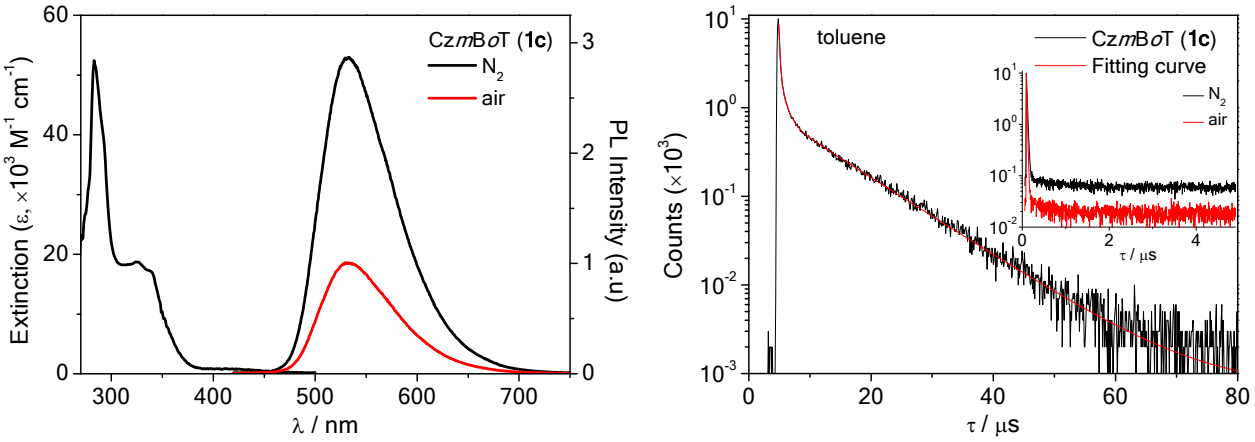

Figure S8. (Left) UV/vis absorption and PL spectra and (right) transient PL decay curves of **1c** in toluene (5.0×10^{-5} M) at 298 K. λ_{PL} = 532 nm. Φ_{PL} (N_2/air) = 0.52/0.13. τ_p (N_2) = 18.5 ns; τ_d (N_2) = 8.92 μs.

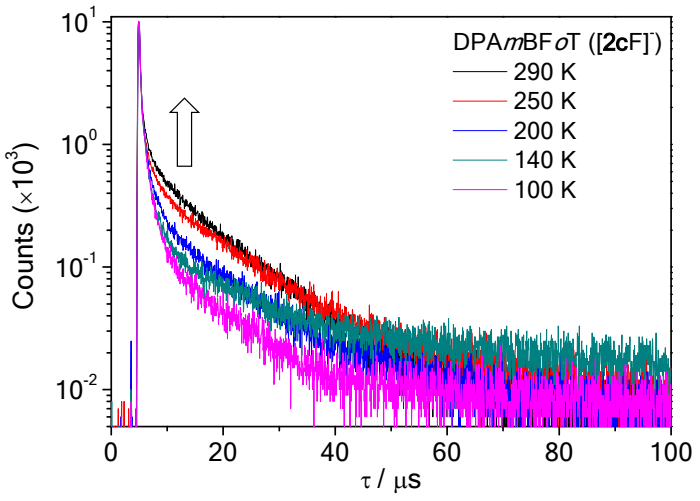

Figure S9. Temperature dependence of transient PL decay curves of [NEt_4][**2c**F] in oxygen-free THF.

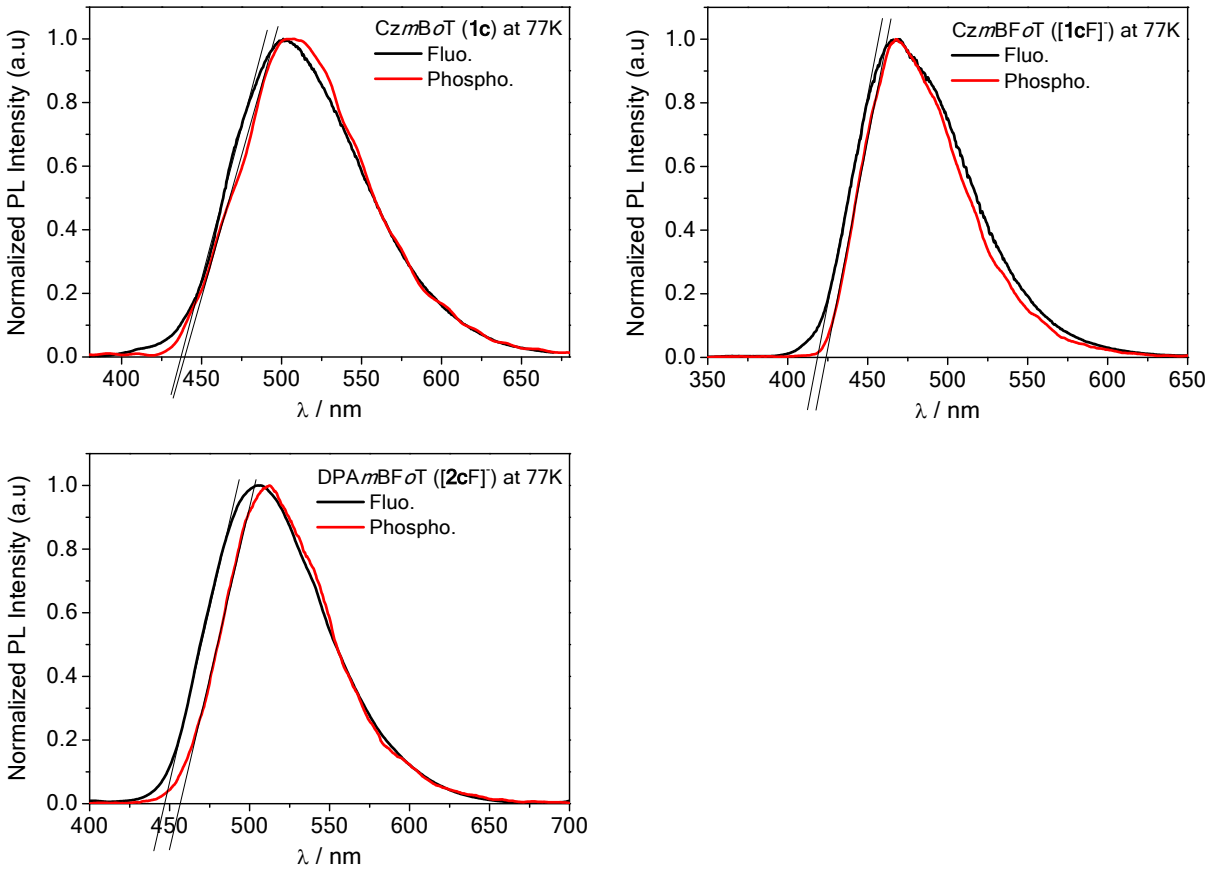

Figure S10. Fluorescence and phosphorescence spectra of **1c**, [NEt_4][**1c**F], and [NEt_4][**2c**F] in THF at 77 K.

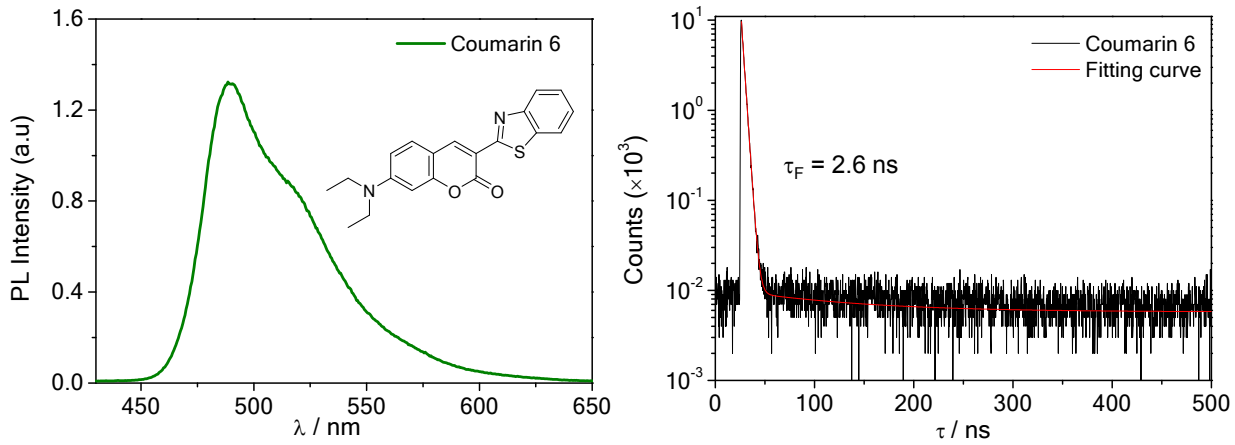

Figure S11. PL spectrum (left) and transient PL decay curve (right) of Coumarin 6 in oxygen-free THF (1.0 μM) at 298 K.

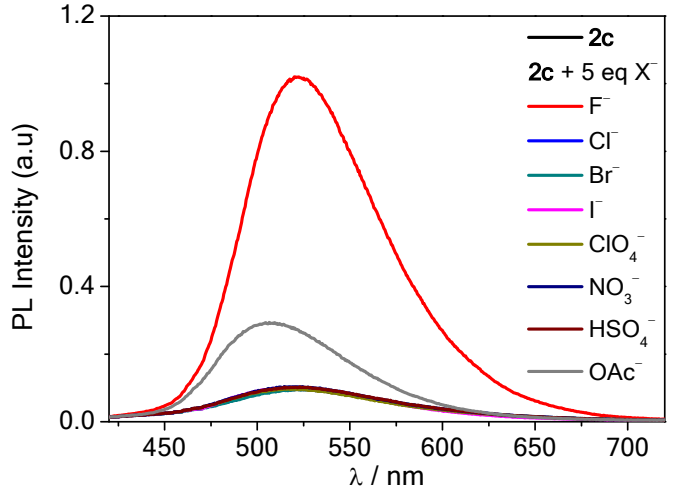

Figure S12. Fluorescence changes of a solution of **2c** (5.0×10^{-5} M in THF) after the addition of 5 equiv of various anions as tetra-*n*-butylammonium salt (λ_{ex} = 367 nm).

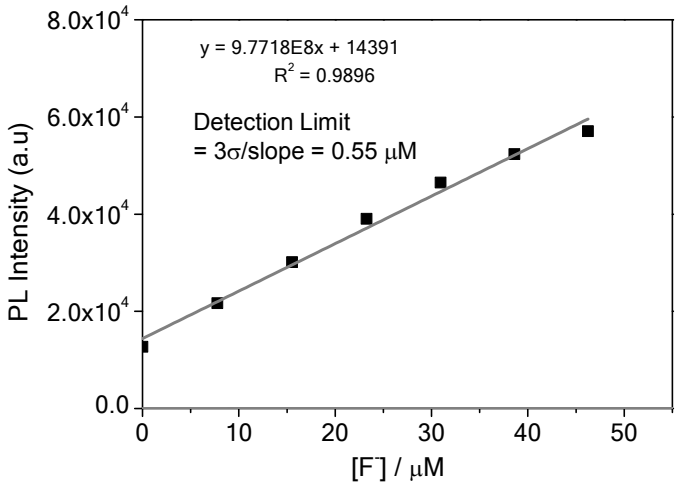

Figure S13. Plot of the fluorescence intensities of **2c** versus the concentration of TBAF in THF.

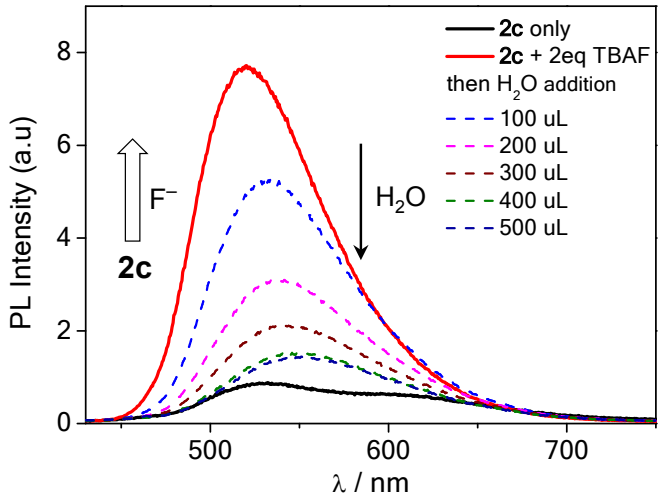

Figure S14. Changes in the fluorescence of **2c** (5.0×10^{-5} M in THF) upon addition of 2 equiv TBAF followed by the incremental addition of water. Note that the presence of water induces a slight solvatochromic shift in the fluorescence.

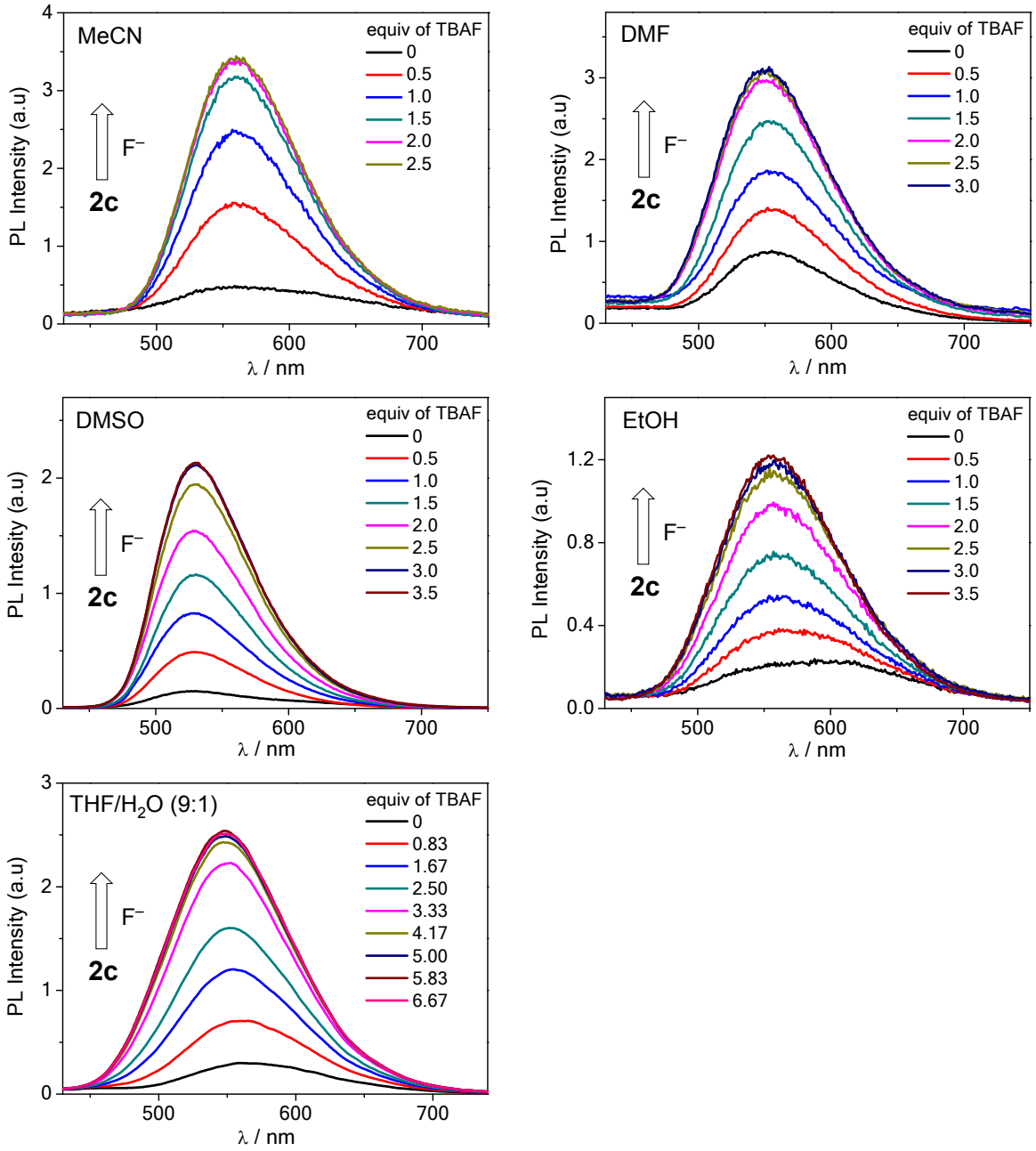

Figure S15. Changes in the fluorescence of **2c** (5.0×10^{-5} M in THF) upon addition of TBAF in various solvents.

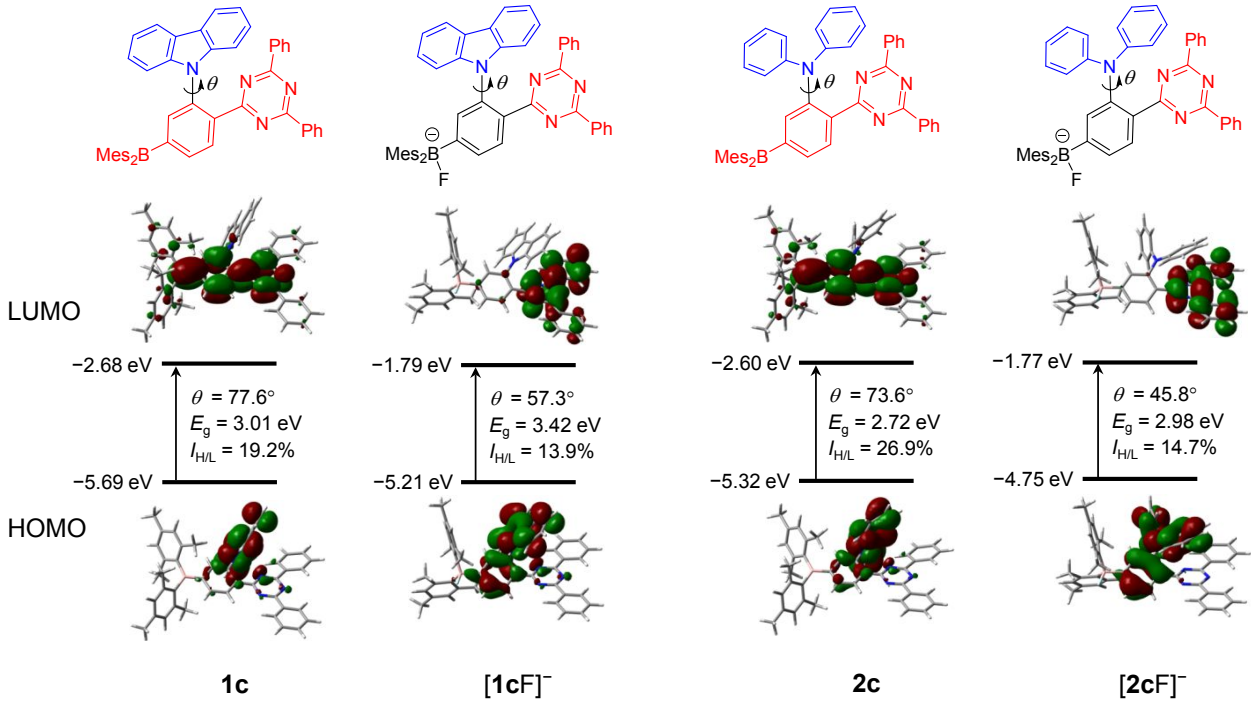

Figure S16. Frontier molecular orbitals, HOMO and LUMO, of (left) **1c** and [**1c**F]$^-$ and (right) **2c** and [**2c**F]$^-$ at their lowest singlet (S_1) excited state geometries from DFT calculations (isovalue = 0.03). The MO energies, dihedral angles (θ, in degrees), band gaps (E_g), and overlap integral extents ($I_{H/L}$) are provided.

Table S2. Molecular orbital energies (in eV) and the contribution (in %) of donor and acceptor moieties to the frontier molecular orbitals at the ground state (S_0) optimized geometries and the overlap integral ($I_{H/L}$, in %) between HOMO and LUMO.

	MO	energy (eV)	donor (Cz or DPA)	acceptor		$I_{H/L}$ (%)
				TzPh	$Mes_2B[F^-]Ph$	
1c (Cz*m*B*o*T)	LUMO	−2.13	1.08	36.45	62.46	23.7
	HOMO	−5.83	92.13	0.84	7.03	
[**1c**F]$^-$ (Cz*m*BF*o*T)	LUMO	−1.47	0.47	99.13	0.40	5.6
	HOMO	−5.30	10.59	0.19	89.22	
2c (DPA*m*B*o*T)	LUMO	−2.04	2.08	39.78	58.14	30.8
	HOMO	−5.45	88.00	0.80	11.19	
[**2c**F]$^-$ (DPA*m*BF*o*T)	LUMO	−1.44	0.56	99.09	0.35	11.9
	HOMO	−5.00	83.94	0.91	15.15	

Table S3. Molecular orbital energies (in eV) and the contribution (in %) of donor and acceptor moieties to the frontier molecular orbitals at the lowest singlet (S_1) excited state optimized geometries and the overlap integral ($I_{H/L}$, in %) between HOMO and LUMO.

	MO	energy (eV)	donor (Cz or DPA)	acceptor		$I_{H/L}$ (%)
				TzPh	$Mes_2B[F^-]Ph$	
1c (Cz*m*B*o*T)	LUMO	−2.68	0.72	35.93	63.35	19.18
	HOMO	−5.69	94.56	1.82	3.62	
[**1c**F]$^-$ (Cz*m*BF*o*T)	LUMO	−1.79	0.57	98.22	1.21	13.88
	HOMO	−5.21	60.34	0.91	38.75	
2c (DPA*m*B*o*T)	LUMO	−2.60	1.73	35.82	62.45	26.87
	HOMO	−5.32	92.60	1.34	6.06	
[**2c**F]$^-$ (DPA*m*BF*o*T)	LUMO	−1.77	1.32	97.87	0.81	14.66
	HOMO	−4.75	70.28	0.67	29.05	

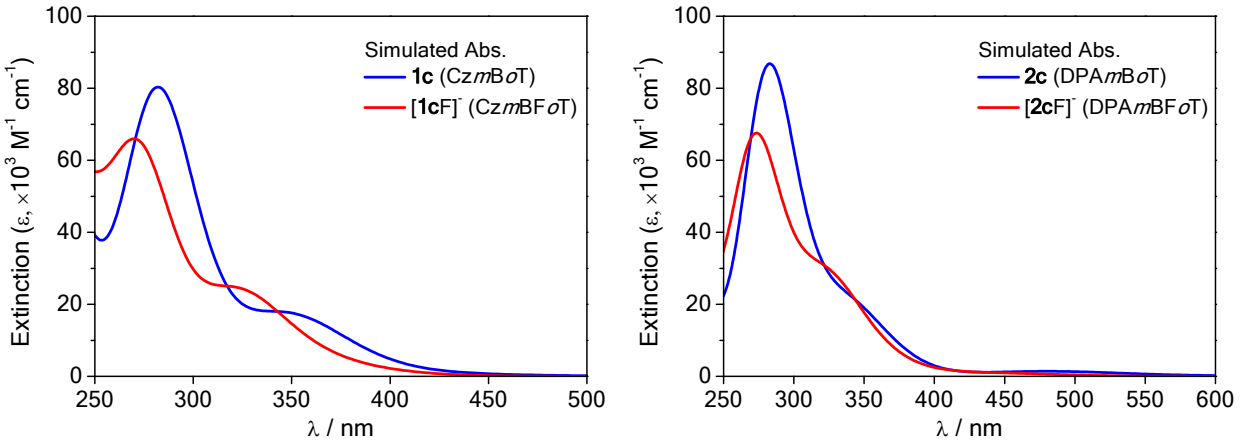

Figure S17. The simulated UV/vis absorption spectra of (left) **1c** and [**1c**F]$^-$ and (right) **2c** and [**2c**F]$^-$.

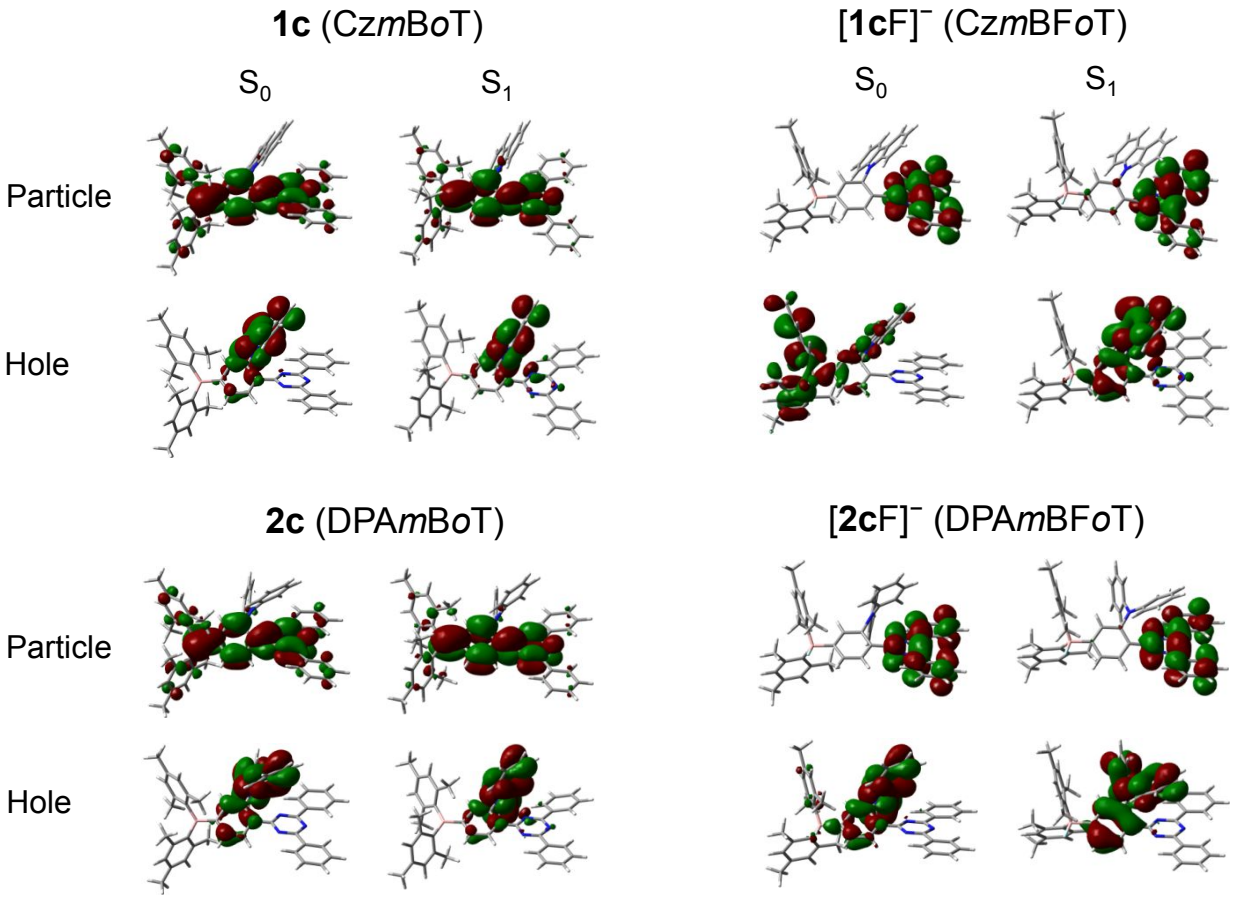

Figure S18. The natural transition orbitals (NTOs), hole and particle, of (top) **1c** and [**1c**F]$^-$ and (bottom) **2c** and [**2c**F]$^-$ (isovalue = 0.02) at their S_0 and S_1 optimized geometries.

Table S4. Computed absorption wavelengths (λ_{abs}, in nm) and corresponding oscillator strength (f_{abs}) for **1c** and [**1c**F]$^-$ from TD-M06 calculations using the M06 geometries at the ground (S_0) fully optimized geometry.

1c			
state	λ_{abs}	f_{abs}	major contribution
S1	431.7	0.0113	HOMO→LUMO (98%)
S2	379.0	0.0031	HOMO→LUMO+1 (99%)
S3	376.5	0.0005	HOMO-1→LUMO (98%)
S4	365.0	0.0934	HOMO-2→LUMO (88%)
S5	349.0	0.2168	HOMO-3→LUMO (89%)
[**1c**F]$^-$			
state	λ_{abs}	f_{abs}	major contribution
S1	390.8	0.0072	HOMO-2→LUMO (26%)
			HOMO-2→LUMO+1 (21%)
			HOMO-1→LUMO (15%)
			HOMO-1→LUMO+1 (12%)
			HOMO→LUMO (12%)
			HOMO→LUMO+1 (13%)
S2	387.8	0.0015	HOMO-2→LUMO (21%)
			HOMO-2→LUMO+1 (22%)
			HOMO-1→LUMO (12%)
			HOMO-1→LUMO+1 (13%)
			HOMO→LUMO (13%)
			HOMO→LUMO+1 (16%)
S3	364.3	0.0533	HOMO-2→LUMO+1 (13%)
			HOMO-1→LUMO+1 (11%)
			HOMO→LUMO (14%)
			HOMO→LUMO+1 (53%)
S4	362.4	0.0114	HOMO-2→LUMO (10%)
			HOMO-1→LUMO (10%)
			HOMO→LUMO (58%)
			HOMO→LUMO+1 (14%)
S5	349.2	0.0006	HOMO-2→LUMO (35%)
			HOMO-1→LUMO (52%)
S6	349.7	0.0031	HOMO-2→LUMO+1 (34%)
			HOMO-1→LUMO+1 (51%)
S7	344.0	0.0010	HOMO-5→LUMO (86%)
			HOMO-5→LUMO+1 (12%)

S8	334.5	0.0051	HOMO-5→LUMO (12%)
			HOMO-5→LUMO+1 (85%)
S9	328.7	0.0025	HOMO-6→LUMO (78%)
			HOMO-3→LUMO (12%)
S10	325.1	0.3794	HOMO-6→LUMO+1 (72%)
			HOMO-3→LUMO+1 (18%)

Table S5. Computed absorption wavelengths (λ_{abs}, in nm) and corresponding oscillator strength (f_{abs}) for **2c** and [**2c**F]$^-$ from TD-M06 calculations using the M06 geometries at the ground (S_0) fully optimized geometry.

2c			
state	λ_{abs}	f_{abs}	major contribution
S1	484.9	0.0291	HOMO→LUMO (98%)
S2	427.6	0.0038	HOMO→LUMO+1 (99%)
S3	359.4	0.0493	HOMO-1→LUMO (31%)
			HOMO→LUMO+2 (62%)
S4	353.9	0.0535	HOMO-1→LUMO (56%)
			HOMO→LUMO+2 (35%)
S5	339.6	0.2466	HOMO-2→LUMO (85%)
[**2c**F]$^-$			
state	λ_{abs}	f_{abs}	major contribution
S1	443.6	0.0136	HOMO→LUMO (63%)
			HOMO→LUMO+1 (36%)
S2	438.5	0.0056	HOMO→LUMO (35%)
			HOMO→LUMO+1 (61%)
S3	362.8	0.0667	HOMO-1→LUMO+1 (89%)
S4	362.0	0.0026	HOMO-1→LUMO (90%)
S5	346.0	0.0003	HOMO-2→LUMO (95%)
S6	344.9	0.0051	HOMO-2→LUMO+1 (94%)
S7	333.8	0.0011	HOMO-5→LUMO (69%)
			HOMO-3→LUMO (17%)
S8	328.1	0.4393	HOMO-5→LUMO+1 (65%)
			HOMO-3→LUMO+1 (22%)
S9	321.0	0.0001	HOMO-5→LUMO (14%)
			HOMO-3→LUMO (80%)
S10	318.5	0.0332	HOMO-5→LUMO+1 (17%)
			HOMO-3→LUMO+1 (73%)

Table S6. The calculated energy splitting between the S_1 and T_1 states ($\Delta E_{ST(ad)}$) and vertical emission wavelength (λ_{em}, in nm) from singlet excited state (S_1) with the corresponding oscillator strength (f_{em}) and reorganization energy (λ_{ROE}).

	$\Delta E_{ST(ad)}$ (eV)	λ_{em}	f_{em}	major contribution	λ_{ROE} (S_0-S_1) (eV)
1c (Cz*m*B*o*T)	0.12	574.7	0.0068	HOMO→LUMO (99%)	0.26
[**1c**F]$^-$ (Cz*m*BF*o*T)	0.11	470.4	0.0096	HOMO→LUMO (83%) HOMO-1→LUMO (15%)	0.01
2c (DPA*m*B*o*T)	0.15	675.1	0.0226	HOMO→LUMO (99%)	0.41
[**2c**F]$^-$ (DPA*m*BF*o*T)	0.10	564.2	0.0026	HOMO→LUMO (99%)	0.21

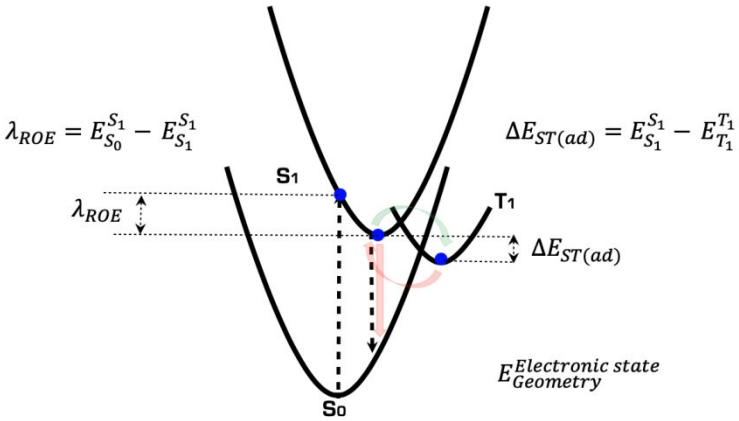

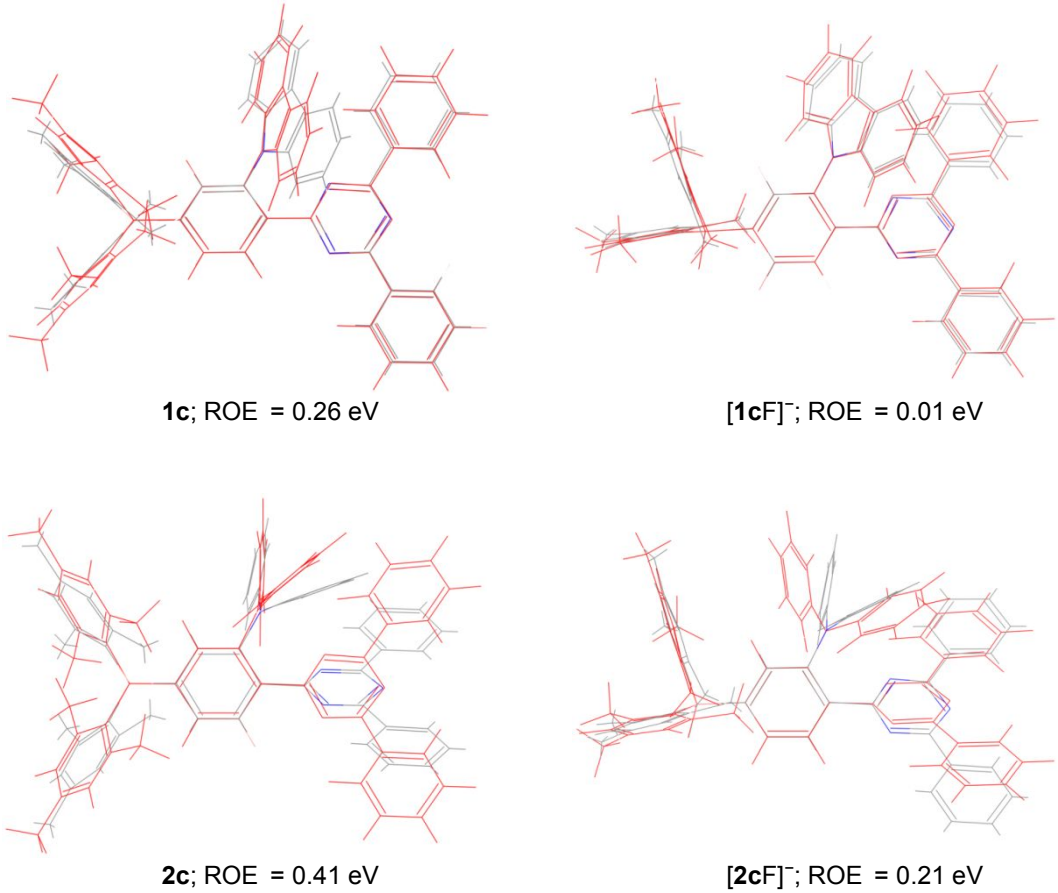

Figure S19. Superimposed optimized geometries of the S_0 and S_1 states with the reorganization energy (ROE). Gray: S_0 geometry; Red: S_1 geometry.